Mechanical analysis and characterization of IGUs with different silicone sealed spacer connections - Part 2: modelling

Chiara Bedon · **Claudio Amadio**

Accepted: 9 June 2020

Abstract Insulated Glass Units (IGUs) typically consist of two glass layers, either monolithic and/or laminated sections, that mechanically interact via an hermetically-sealed air (or gas) cavity, and a series of linear spacer connections along their edges. In this paper, based on the experimental tests for small-scale IGU joints under pure shear and IGU prototypes in bending discussed in "Part I", a special care is spent for the Finite Element (FE) numerical characterization and analysis of these composite systems, with a focus on the actual mechanical properties and load-bearing mechanism for the involved components. Major advantage is taken from the full 3D solid geometrical description of the connection components and the gas cavity infill. The actual role of both primary and secondary sealant layers is first assessed. Further support is derived from analytical calculations for the connection efficiency assessment, based on the adaptation of simplified formulations of literature. Finally, a calculation example is proposed to assess the magnitude of load sharing phenomena, based on FE numerical and analytical calculations for selected configurations.

Keywords Insulated glass units (IGUs) · Spacer connections · Finite element (FE) numerical modelling · Analytical formulations

C. Bedon (✉)· C. Amadio
Department of Engineering and Architecture, University of Trieste, Piazzale Europa 1, 34127 Trieste, Italy
e-mail: chiara.bedon@dia.units.it

1 Introduction

Insulated Glass Units (IGUs) are largely used in buildings for several advantages, but are still not well known from a pure mechanical point of view. Compared to other glazing systems, a combination of multiple mechanical and thermal aspects should be in fact taken into account for their load-bearing performance assessment. So far, however, only few research studies have been spent for specific mechanical issues of IGUs, see for example Morse and Norville (2016), Bedon and Amadio (2018a, b), McMahon et al. (2018). In this regard, it is generally recognized that Finite Element (FE) numerical models or simplified analytical formulations can both support the detection of optimal design configurations. On the other side, it is also known that several key input parameters should be accurately defined and calibrated, for reliable stress/displacement estimates. This is the case of glass structures in general, but especially of IGUs, due to the presence of linear edge spacer connections and an interposed cavity infill that can react to various ambient variations, thus requiring extensive investigations in support of reliable FE assumptions (Buddenberg et al. 2016).

This paper follows and extends the experimental investigation reported in a previous "Part I", see Bedon and Amadio (2020), and specifically focuses on the mechanical characterization of IGU components based on FE numerical studies (ABAQUS; Simulia 2020). For both pure shear or bending loading configurations, the

actual role of primary and secondary seals on the overall load-bearing performance of IGUs under short-term loads is first explored. For sake of clarity, the numerical analyses are divided for shear tests on small-scale IGU joints (Sect. 2), bending of 2-edge sealed IGU specimens (Sect. 3) and bending of 4-edge sealed IGU specimens, thus inclusive of the gas cavity infill (Sect. 4). Additional support to the comparative calculations is derived from analytical models summarized in Bedon and Amadio (2020), and being respectively referred to composite beams with flexible mechanical connection (i.e., the γ-method adapted from Möhler 1956) or to sandwich beam-like assemblies with adhesive bonding (extended from Pascual et al. 2019).

In conclusion, see Sect. 5, the reliability of simplified analytical formulations provided in prEN 13474-1 (2007), CNR DT 210 (2013) to account for load sharing phenomena is also preliminary assessed. The actually available load sharing formulations are in fact specifically recommended for IGUs with four linear supports along all the edges, and subjected to uniform distributed pressures. While these boundary and loading configurations are certainly of interest for design purposes, however, they do not reflect the high variability of possible operational conditions for IGUs in buildings. For the case-study configuration reported in Sect. 5, both the boundary configurations of four or two (shortest) linearly supported edges are taken into account for IGUs under external uniform pressures. Both FE numerical and simplified analytical stress and deflection estimates are compared for the constituent glass panels, giving evidence of major variations.

2 FE numerical analysis of IGU joints in shear

2.1 Methods

The preliminary FE model ("FE-S0nom", in the following) was assembled in ABAQUS (Simulia 2020) to describe the nominal geometry of the test specimen (triplet shear sample) schematized in Fig. 1, and inclusive of $n_{edges} = 4$ spacer connections composed of:

- WE bar (CHROMATECH Ultra®16 – Version F (AluPro)),
- butyl primary seal (Butylver®), and
- silicone bond for the secondary seal (DOWSIL^{TM} 3363).

The simulations were carried out with the ABAQUS/Explicit solver, so as to facilitate the convergence of analyses in the damaged stage. Geometrical nonlinearities were taken into account. As usual, displacement-control simulations in a quasi-static regime under the monotonic increase of imposed deformations were ensured by controlling the energy balance of the whole system. The overall loading strategy was set to capture the reference experimental setup (with 1 mm/min the imposed displacement rate in Bedon and Amadio 2020). The monotonic increasing displacement for the shear triplet was uniformly distributed on the top face the middle glass panel ("Glass 2"). At the same time, a linear base restraint was assigned to the bottom face of the external "Glass 3". Additional symmetry restraints were taken into account as schematized in Fig. 2. For symmetry, the computational cost of analyses was in fact minimized by considering 1/4th the specimen geometry in Fig. 1.

In order to capture in detail the mechanical interaction of the involved components under pure shear deformations, a set of 8-node brick elements (C3D8R type from ABAQUS library) were used to reproduce each FE joint specimen. These included (for 1/4th the experimental sample) two glass panels, one silicone layer, two butyl layers and the WE spacer bar. Careful consideration was thus spent for the detection of reliable FE modelling assumptions, but aiming at privileging a simplified geometrical description of joint details. As known, spacer connections have a key role on the assessment of IGU behaviours under both mechanical or climatic loads. The mathematical and/or FE assumptions, accordingly, should properly reflect the actual response and reciprocal interaction of the involved components. Differing from Buddenberg et al. (2016), where equivalent tension springs calibrated to experimental climatic loads were proposed for the linear edge seals, a more refined FE description (but still in presence of certain approximations) was adopted in this paper for the connection components.

In the case of the WE spacer bar in Fig. 1c, in particular, a simplified box-shaped cross-section was taken into account for numerical purposes (0.1 m the uniform thickness, with 15.5 mm × 6.5 mm the external size), and used in place of the nominal corrugated profile. Accordingly, butyl and silicone strips were schematized in the form of adhesive strips with rectangular cross-sections, see Fig. 2.

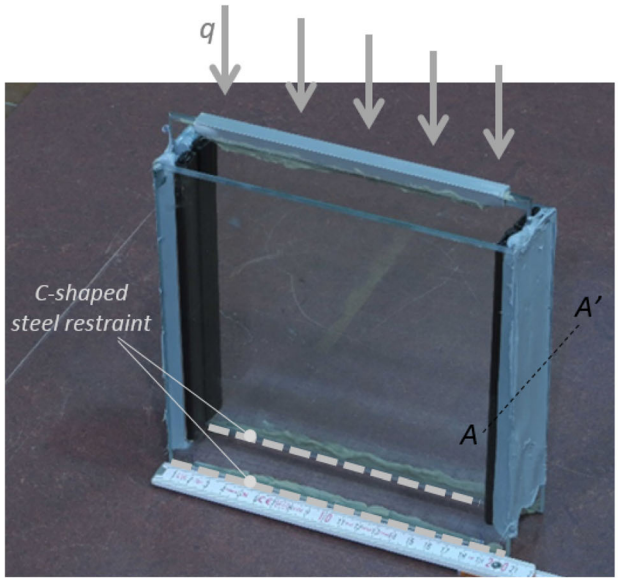

a

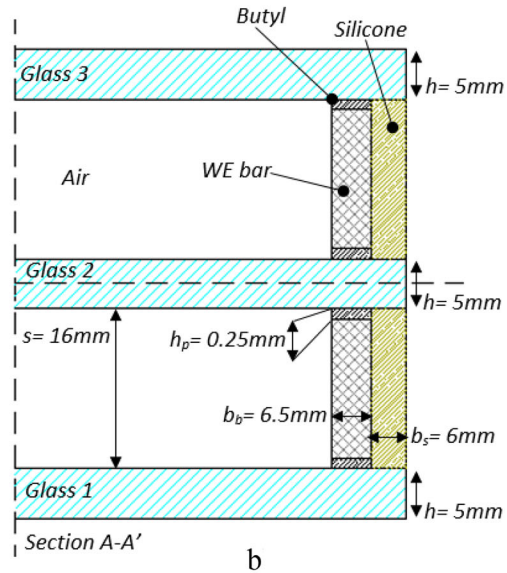

b

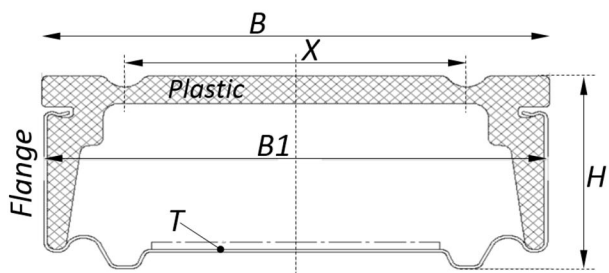

c

CHROMATECH Ultra® 16 – Version F (AluPro)	
H (mm)	6.9 (± 0.15)
Flange (mm)	5.1 (± 0.1)
B (mm)	15.6 (± 0.15)
B1 (mm)	15.5 (± 0.15)
X (mm)	10.45 (± 0.1)
T (mm)	0.1

Fig. 1 Small-scale IGU joint specimen: **a** axonometry and **b** schematic transversal cross-section (detail), with **c** nominal geometry for the WE bars in use. (reproduced from www.alupro.it)

Besides these geometrical simplifications, the computational efficiency of FE simulations was still affected by mesh features. The mesh pattern consisted in fact of a series of variable edge-size brick elements, with a strongly refined scheme in the region of the spacer connection (butyl layers and bar). To avoid locking issues, the minimum edge size was set in 0.1 mm. In the case of the connection components, due to their nominal geometry, such a minimum size was used for a regular mesh pattern. For the glass panels only, the minimum size of 0.1 mm was kept constant in the thickness of the panels, along the lateral edges of each specimen. The same edge size was then progressively increased, thanks to a variable mesh scheme, with a reference size up to 2.5 mm for the brick elements belonging to the portions of glass not in contact with the spacer connection (i.e., central region).

2.2 Mechanical interactions and material properties

The characterization of load-bearing members and the reciprocal interaction between the involved components was mainly based on past experimental observations reported in Bedon and Amadio (2020) and literature efforts. The major challenge was represented by the sealant layers, being responsible of the overall mechanism for the assembled IGUs and of the activation of a composite bending response. As known, the rubbering bonds in use for spacer connections, are typically characterized by a viscoelastic behaviour that is sensitive both to time loading and temperature conditions (see for example Wolf 2002, 2003). Service-life operational conditions can then further affect the nominal material properties, thus manifest in additional degradation mechanisms for IGU systems. Accord-

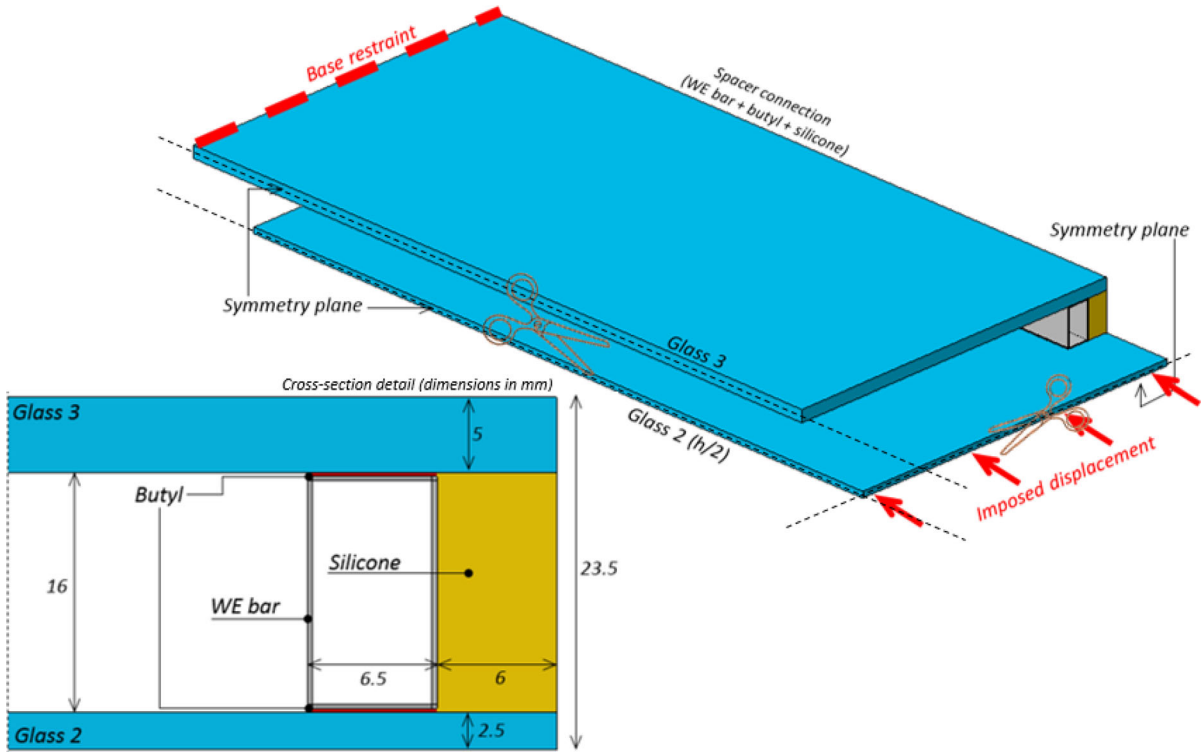

Fig. 2 Reference FE model (1/4th the nominal geometry) of a IGU joint under shear loads (ABAQUS)

ingly, refined studies should be generally carried out based on the accurate knowledge of the viscous parameters for the compound in use (Liang and Mackley 1994; Turowec and Gillies 2016; Sharma and Bhattacharya 2019). Many other influencing parameters to assess could be then represented by the surface properties, dimensions, ageing effects, etc. (Machalicka and Eliasova 2016).

On the other side, in the field of structural glass applications, it is also recognized that equivalent material properties can be often used to obtain reliable stress-strain estimates of bonded systems. This is also the case of simple laminated glass sections, where the interlayer foils in use to provide a certain shear coupling to glass panels can be efficiently described (as far as degradation and delamination phenomena are disregarded Dural 2016; Bedon 2019) in the form of equivalent secant moduli that are specifically referred to a given time loading and temperature configuration (Haldimann et al. 2008; CNR DT 210 2013; Hänig et al. 2019; Kuntsche et al. 2019). Finally, see Koslowski and Wolf (2016), primary seals have negligible structural roles in IGU assemblies.

Compared to more refined FE approaches, the herein preferred modelling assumption consisted in the use of a "tie" constraint for all the involved interfaces (i.e., glass-butyl, glass-silicone, butyl-bar, silicone-bar and butyl-silicone), thus assuming an ideal bond enabling possible relative deformations for the surfaces of interest. At the same time, however, such a constraint choice was supported by an accurate mechanical characterization of materials, so as to capture the overall shear response of the joint specimens discussed in Bedon and Amadio (2020), as well as the IGU specimens in bending (see Sect. 3). Rigid "tie" constraints, are in fact reasonably accepted to represent reliable bonding interfaces for structural glass applications, both at the laminated section level (i.e., glass-interlayer interface) or in terms of adhesive joints. Past literature studies focused on the numerical investigation of structural glass components and systems (i.e., hybrid beams or panels) with adhesively bonded members proved that "tie" constraints can be efficiently combined with reliable constitutive laws for the bonding materials in use, and offer rather accurate global estimates especially for mechanical systems under short-term loads. Certainly,

Table 1 Input mechanical properties for FE modelling of small-scale IGU joints in shear ("FE-S0nom" model)

Material	E (MPa)	$\nu(-)$	f_y (MPa)	f_u (MPa)	ρ (kg/m^3)
Glass[(1)]	70000	0.23	–	–	2490
Butyl[(2)]	0.56	0.49	0.25	0.25	600
Silicone[(3)]	4.80	0.49	1.50	1.50	1100
Stainless steel[(4)]	197000	0.3	360	750	7800

Key: values from (1) EN 572-2 (2004); (2) Turowec and Gillies (2016); (3) www.dow.com; (4) EN 10088-2: (2014)

a generalized discussion of major outcomes summarized in this paper should be based on FE assumptions integrated by more refined surface interactions (i.e., Cohesive Zone Modelling (CZM) approaches for adhesively bonded connections in glass) and viscous constitutive laws for the sealant layers, so as to include progressive damage phenomena of destructive simulations (see for example Bedon et al. 2018; Katsivalis et al. 2019).

Careful consideration was thus paid for the mechanical features of the selected IGU components. At a first attempt ("FE-S0nom" model), the nominal properties reported in Table 1 were taken into account. A linear elastic behaviour was considered for glass, given that an elastic, rigid-body translation was expected for the plates under the imposed shear setup of Fig. 1. Accordingly, through the post-processing stage, stress peaks in the glass plates were monitored and compared with nominal tensile bending resistance values, to ensure the reliability of FE results. At the same time, three equivalent, ideal elasto-plastic stress-strain constitutive laws were used for steel (spacer bar), DOWSIL^{TM} 3363 silicone and Butylver®. Worth of interest in Table 1 is the relatively low resistance of primary seal, thus enforcing its negligible load-bearing contribution and the use of a rigid "tie" constraint, in place of more expensive CZM techniques (whose input characterization would require additional local and global experimental measurements).

2.3 Experimental characterization of silicone and reference FE configurations

At a final stage of the FE modelling procedure, the attention was focused on possible case-study configurations of technical interest, with respect to the experimental outcomes reported in Bedon and Amadio (2020). These included variations in geometrical and/or mechanical assumptions.

Among others, differing from Table 1, the equivalent mechanical stiffness and resistance of silicone were calibrated from the experimental shear estimates of IGU joints in Fig. 1. At the time of the shear experiments, it was in fact pointed out that both the butyl and silicone layers are responsible of the actual bonding (and thus load-bearing capacity) for the tested small-scale spacer connections. However, the butyl layer was recognized to have a marginal contribution for structural purposes, and the response of the silicone layers was experimentally associated to an equivalent material with:

$$G_{joint} = \frac{s \cdot K_{joint}}{2 \cdot A_{bond}} = 2.16\,\text{MPa} \quad (1)$$

$$E_{joint} = G_{joint}\,(2 \cdot (1 + \upsilon_s)) = 6.44\,\text{MPa} \quad (2)$$

the elastic moduli, with $\nu_s = 0.49$, where:

$$\tau_{joint} = \frac{F_{joint}}{n_{bond}} \cdot \frac{1}{A_{bond}} = 1.84\,\text{MPa} \quad (3)$$

is the ultimate shear resistance.

In Eqs. (1)–(3), $s = 16$ mm is the silicone height (and cavity thickness, see Figs. 1 and 2), $n_{bond} = 2$ represents the number of shear resisting surfaces and A_{bond} is the corresponding area (for a single silicone strip), while:

- K_{joint} in Eq. (1) is the experimental serviceability stiffness of a single spacer connection (i.e., detail of Fig. 2), with:

$$K_{joint} = \frac{K_{ser}}{n_{edges}} = 0.292\,\text{kN/mm} \quad (4)$$

- and K_{ser} in Eq. (4) represents the experimental serviceability stiffness of the IGU specimen (composed of $n_{\text{edges}} = 4$ representing the number of spacer connections according to Fig. 1),

Finally:

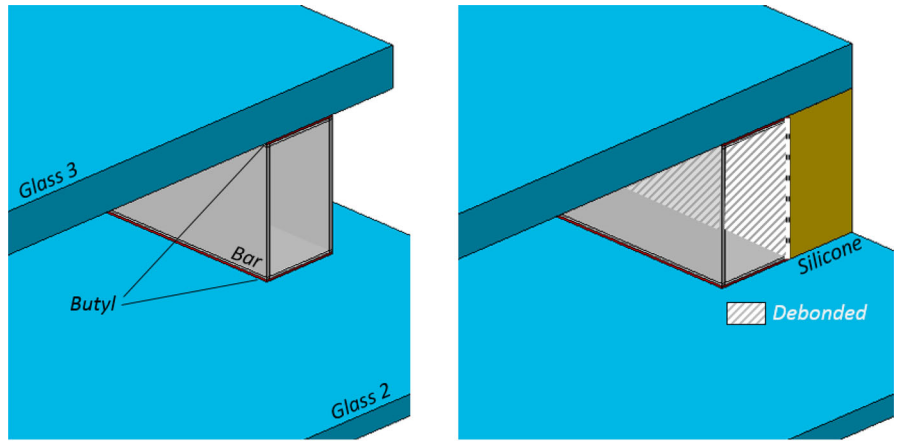

a FE-S1 (without silicone bond) b FE-S2 (debonded silicone)

Fig. 3 Schematic representation of connection detailing for the FE parametric study (ABAQUS)

– F_{joint} in Eq. (3) is the ultimate resistance of a single spacer connection, with

$$F_{joint} = \frac{F_{shear}}{n_{edges}} = 1.0125\,\text{kN} \tag{5}$$

– and F_{shear} in Eq. (5) denotes the experimental ultimate resistance of the IGU specimen ($n_{\text{edges}} = 4$),

In addition to the experimental derivation of material properties for the silicone layers, a careful consideration was spent on the actual quantification of stiffness and resistance contributions due to the same silicone strips. Further consideration was finally paid to numerically assess the possible mechanical interaction between the silicone layers and the adjacent spacer bar (lateral surface), so as to indirectly account for possible uncertainties on adhesion or production defects. Accordingly, the FE investigation on IGU joint specimens in shear was thus extended so as to include different geometrical and mechanical configurations of technical interest for sensitivity analysis of past experiments, and being representative of:

(a) FE-S0nom: geometrical system of Fig. 2, with nominal mechanical properties for all the materials (Table 1);
(b) FE-S0: the same of case a), but with experimentally derived mechanical properties for the silicone layers (see Eqs. 1–3);
(c) FE-S1: as in case b), but removing the silicone layer (spacer bar + butyl layers only), see Fig. 3a;
(d) FE-S2: the same of case b), but with an imposed debond for the silicone-to-bar interface (Fig. 3b).

2.4 Results

The analysis of FE results herein reported was mainly focused on the evolution of stress peaks in the bonding layers for IGU joints agreeing with Fig. 2, so as to assess their load-sliding response at different load levels. Actually, besides the simplicity of the reference FE configuration described in Fig. 2, the numerical investigations allowed to capture some relevant aspects of the IGU joint performance.

Moreover, the FE models generally proved to capture with accuracy the overall shear response of the tested IGU joint specimens. The FE-S0nom in Fig. 4a, for example, gave evidence of a load-sliding mechanism in shear that mostly fits with the experimental measurements. Even more accurate correlation was obtained from the FE-S0 system in Fig. 4a, with experimentally derived silicone properties.

The support of such a kind of FE predictions was thus further exploited to detect the relevant joint stiffness parameters, as a function of the stress peaks in the bonding layers (butyl and silicone respectively). The typical FE response was in fact generally characterized by three different stages, namely represented by:

– *Stage I*: initial elastic response, with both the butyl and silicone layers in the elastic regime;
– *Stage II*: first yielding of butyl layers, with the progressive transmission of the load-bearing capacity from the butyl layers to the silicone strip;
– *Stage III*: yielding of the silicone layer, with achievement of the ultimate resistance for the whole FE system.

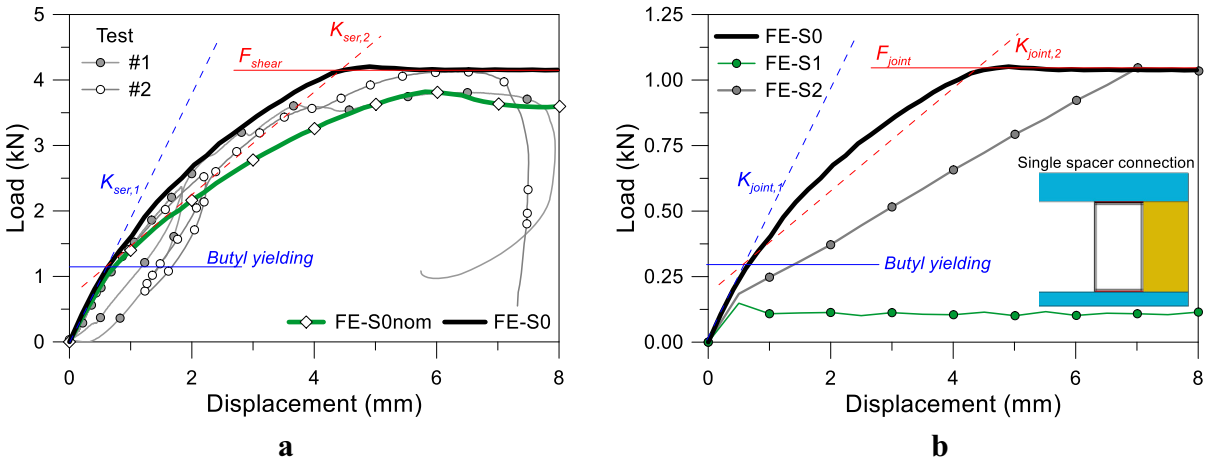

Fig. 4 Shear performance assessment of IGU joints (ABAQUS): stiffness estimates for **a** whole IGU specimens ($n_{edges} = 4$), with experimental measurements from Bedon and Amadio (2020), or **b** single spacer connections (sensitivity study)

Table 2 Calculation of shear performance parameters for single spacer connections according to Fig. 4b

FE model #	$K_{\text{joint},1}$ (kN/mm)	$K_{\text{joint},2}$ (kN/mm)	F_{joint} (kN)	$\Delta K_{\text{joint},1}$ (%)	$\Delta K_{\text{joint},2}$ (%)	ΔF_{joint} (%)
FE-S0	0.458	0.187	1.035	–	–	–
FE-S1	0.296	–	0.115	− 35.37	–	− 88.89
FE-S2	0.365	0.135	1.020	− 20.31	− 27.81	− 1.45

As far as the shear performance assessment is carried out in terms of full specimen (with $n_{edges} = 4$ spacer connections), see Fig. 4a, the above stages I-to-III basically correspond to a joint stiffness that can be expressed as:

- $K_{\text{ser},1}$: initial stiffness for the whole IGU specimen, calculated under the limit condition that the butyl layers first yield;
- $K_{\text{ser},2}$: plastic stiffness of the whole IGU specimen calculated under the limit condition that the silicone layers also yield.

In order to collect some generalized numerical outcomes of technical interest, however, it is convenient to investigate a single spacer connection, and focus on the actual contribution of silicone layers. Such an approach leads to the definition of stiffness parameters $K_{\text{joint},1}$ (elastic stage) and $K_{\text{joint},2}$ (plastic stage) that are in correlation with $K_{ser,1}$ and $K_{ser,2}$ defined above. This corresponds to the load-sliding responses in Fig. 4b and to stiffness parameters listed in Table 2. There, absolute values from the FE models herein explored are reported. In addition, percentage scatter values are proposed, with respect to the FE-S0 assembly that better captures the experimental results.

Worth of interest in Fig. 4b and Table 2 is the FE-S1 initial response (no silicone bonds). On one side, it is in fact generally recognized that the primary butyl layers are conventionally regarded as non-structural components. However, they are clearly responsible of the composite action activation for the examined IGU assembly (at least for limited load levels), and thus of the initial joint stiffness estimates ($K_{joint,1}$). Such a FE outcome is also in close correlation with Starman et al. (2020), were it was numerically proved that the primary seals in cold conditions and under short term loads are responsible for relevant stiffness contributions. On the other hand, see Table 2, the ultimate resistance of spacer connections is primarily offered by silicone layers (up to the ≈90% of total estimates).

For both the elastic and plastic stages, further relevant considerations can be derived for the adjacent silicone layers. The FE studies herein summarized proved that the shear stiffnesses $K_{joint,1}$ and $K_{joint,2}$ are affected not only by the silicone features (size and rigidity), but also by its possible bonding interaction

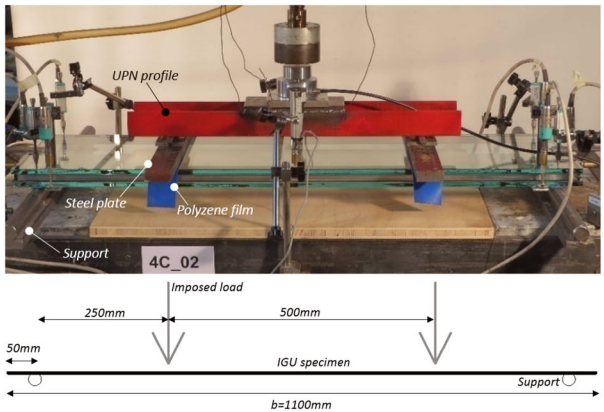

a

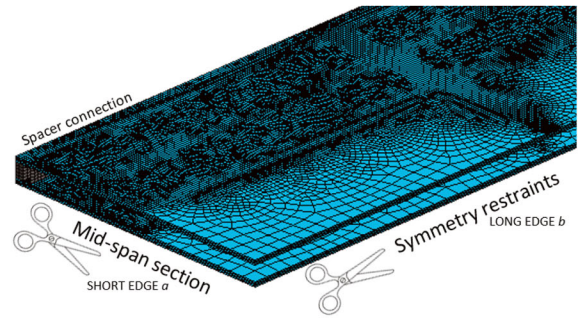

b

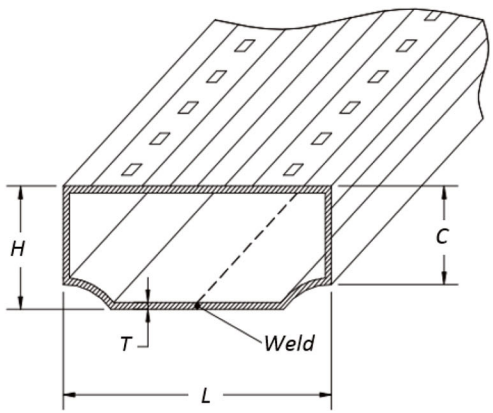

c

Aluminum spacer H65® – Profile A155 (AluPro)

L (mm)	15.50 (± 0.1)
H (mm)	6.50 (± 0.1)
C (mm)	5.10 (± 0.2)
T (mm)	0.31 (± 0.01)

Fig. 5 Bending performance assessment of IGU panels: **a** reference test setup and **b** FE model detail (ABAQUS), with **c** AL spacer bar in use. (reproduced from www.alupro.it)

with the lateral spacer bar. Such an outcome can be recognized by the comparison of the FE-S0 or FE-S2 results in Fig. 4b and Table 2. Disregarding that the bar web and the silicone layer are mechanically interconnected, the FE-S1 results show that the spacer connection would obtain a minimum stiffness increase, compared to FE-S1 estimates. First, the butyl layers are in fact responsible to carry-on most of the imposed shear deformations. The limited resistance of butyl layers, however, vanishes for small imposed deformations, and such a limit condition activates the transmission of imposed loads from "damaged" butyl to the adjacent silicone layer, thus resulting in a certain residual stiffness ($K_{\text{joint},2}$) and ultimate resistance (F_{joint}). The shear performance of the spacer connection in Fig. 4b totally modifies, with enhanced stiffness improvement, as far as the silicone joint is fully bonded with the spacer bar, see FE-S0.

3 FE numerical analysis of 2-edge sealed IGUs in bending

3.1 Methods

Following Sect. 2, the reference geometry and four-point bending test setup schematized in Fig. 5a was taken into account for the analysis of IGU samples. Modelling methods and assumptions were kept qualitatively identical to Sect. 2, with the exception of trivial variations in the boundary and loading conditions, as well as interactions (i.e., for the gas cavity infill). The bending performance assessment was carried out in the form of displacement-controlled simulations in a quasi-static regime. The imposed bending loads were applied through distributed pressures reproducing the setup of Fig. 5a, and linearly increase up to the failure stage for each one of the selected specimens.

Table 3 Four-point bending tests (group I, with $a = 400\,\text{mm} \times b = 1100\,\text{mm}$)

Series	Test repetitions	Label	h (mm)	Spacer bar	Seal type	Sealed edges in total	Secondary seal (no. of sealed edges), b_s (mm)
2C	1	2C_01	5	AL	P	2	X
2C2S	1	2C2S_01	5	AL	P + S	2	Y (2), 9

Key: *AL* aluminum, *WE* warm edge, *P* primary seal (Butylver 0.25 mm), *S* secondary seal (DOWSIL 3363 silicone), *Y* yes, *X* no

For double symmetry, 1/4th of the nominal geometry for both the 2C2S_01 and 2C_01 bending IGU specimens with $h_1 = h_2 = h = 5\,\text{mm}$ thick glass panels and early discussed in Bedon and Amadio (2020) was numerically reproduced, with appropriate restraints (see Fig. 5b and Table 3). In order to minimize possible uncertainties in the comparison of FE and past experimental estimates (and especially the actual bending stiffness of WE bars in Fig. 2), the attention was mainly focused on specimens with AL spacer bars (see Fig. 5c). The latter was described in the form of a regular box section (0.31 mm the uniform thickness, with 15.5 mm × 6.5 mm the external size), that well adapts to the nominal geometry.

C3D8R solid elements from ABAQUS library were used. As in Sect. 2, a regular mesh scheme was used for the spacer connection components, while a variable pattern was preferred for the glass panels. The refinement in the region of the external edges (i.e. for the bonding layers, the spacer bars and the perimetral portions of glass) typically resulted in 250,000 brick elements and 800,000 DOFs for each FE assembly (see Fig. 5b).

3.2 Mechanical interactions, material properties and reference configurations

All the mechanical interactions for the involved FE components were defined as in the case of shear triplets (i.e., with surface-distributed "tie" constraints). The presence of 2-edge sealed panels facilitated the numerical assembly and allowed to disregard potential load sharing phenomena due to unsealed cavity.

Regarding the mechanical characterization of materials in use, based also on Sect. 2, nominal silicone properties were disregarded, in place of the more accurate experimentally derived properties that were directly implemented in ABAQUS (see Eqs. 1–3). Glass and butyl were indeed still described as in Table 1. The use of a linear elastic material for AN glass, in this regard, was justified by the major focus on the pre-fracture numerical analysis of bending responses. At the same time, such an assumption was recommended due to the severe scatter and variability in the actual tensile resistance of AN glass, thus in the high variability that could have affect the experimental fracture patterns. Through the post-processing stage of FE results and corresponding experimental deformations, accordingly, the evolution of tensile stresses along the restrained edges of glass was specifically investigated (being representative of the fracture origin for all the experimental samples). Finally, an equivalent elasto-plastic constitutive law was used for the AL spacer bar. According to EN 573-3 (2019) and EN 485-2 (2016) product standards, the mechanical parameters were set equal to $E_{al} = 70\,\text{GPa}$, $f_{y,al} = 160\,\text{Mpa}$ and $f_{u,al} = 195\,\text{MPa}$, with $\varepsilon_{u,al} = 9\%$ the nominal elongation at failure and $\rho_{al} = 2721\,\text{kg/m}^3$.

Three reference FE system options were thus taken into account for bending performance assessment of 2-edge sealed panels:

(a) FE-B0: all the interfaces with ideal "tie" constraint, with nominal mechanical properties for the materials (Table 1), with the exception of silicone (experimental features from Eqs. 1–3). Such a reference FE system was used to represent the 2C2S_01 specimen of Table 3;
(b) FE-B1: the same of case a), but deprived of the silicone layers (thus including only spacer bars + butyl strips). This FE model was implemented to describe the 2C_01 specimen of Table 3, with connection details in analogy with Fig. 3a;
(c) FE-B2: as a further configuration of technical interest, the FE assembly was described as for case a), but without any mechanical connection between the silicone layer and the adjacent spacer bar (Fig. 3b).

3.3 Load-deflection results

As shown in Fig. 6a, the tested configurations offered a useful feedback on the actual bending performance

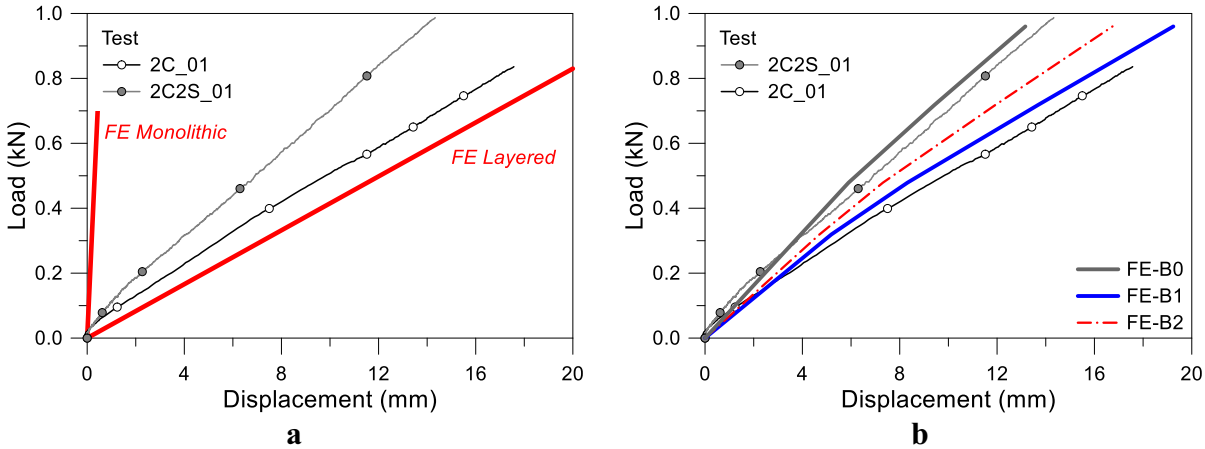

Fig. 6 Bending performance assessment of 2-edge sealed IGU panels (ABAQUS): **a** FE limit conditions and **b** detailed estimates, compared to the past experimental results (Bedon and Amadio 2020)

Table 4 Bending stiffness assessment for the selected IGU panels in Fig. 6b

FE model	$EI_{\text{eff},1}$ (kN/mm)	$EI_{\text{eff},2}$ (kN/mm)	$\Delta EI_{\text{eff},1}$ (%)	$\Delta EI_{\text{eff},2}$ (%)
FE-B0	0.0812	0.0633	–	–
FE-B1	0.0615	0.0456	− 24.26	− 27.96
FE-B2	0.0679	0.0533	− 16.38	− 15.80

of IGU specimens. Compared to the FE limit conditions associated to weak (*layered*) or fully rigid (*monolithic*) connection between the glass edges, the selected specimens clearly show a medium/poor degree of connection, for the 2C2S and 2C series respectively, thus enforcing the positive contribution of silicone layers.

Detailed comparison are collected in Fig. 6b, where it is worth of interest to notice the rather close correlation between the two specimens and the corresponding FE models. For the intermediate FE-B2 configuration (lateral debonding for the silicone layer), a sensitive variation of bending stiffness can be perceived, when compared to the ideal FE-B1 system.

From Fig. 6, a significant variation in the slope of load-deflection curves can be also appreciated, for the past experiments as well as (even less pronounced) corresponding FE models. The latter was found to be numerically associated to the progressive yielding of butyl layers, and thus by the consequent activation (if any) of the silicone layers. In analogy with Sect. 2, it can rationally detected a bending stiffness parameter denoting:

- $EI_{\text{eff},1}$: the initial elastic response of a given IGU panel (up to the first yielding of butyl layers), and
- $EI_{\text{eff},2}$: the plastic bending stiffness of the system (up to fracture f glass, or failure of silicone bonds).

Table 4 shows the so calculated performance parameters, with the percentage variation with respect to the ideally bonded FE-B0 assembly.

3.4 Stress results

As shown in Fig. 6a, the tested configurations proved to offer useful feedback on the actual bending performance of IGU specimens. Compared to the FE limit conditions associated to weak (*layered*) or fully rigid (*monolithic*) connection between the glass edges, the selected specimens offered an intermediate bonding level. Values in Table 4 are inclusive of spacer connection features but also glass stiffness contributions, as well as possible uncertainties in the actual bonding behaviour of the involved components. For the examined scenarios, however, they can provide a first quantification of sealant roles. The same bending stiffness

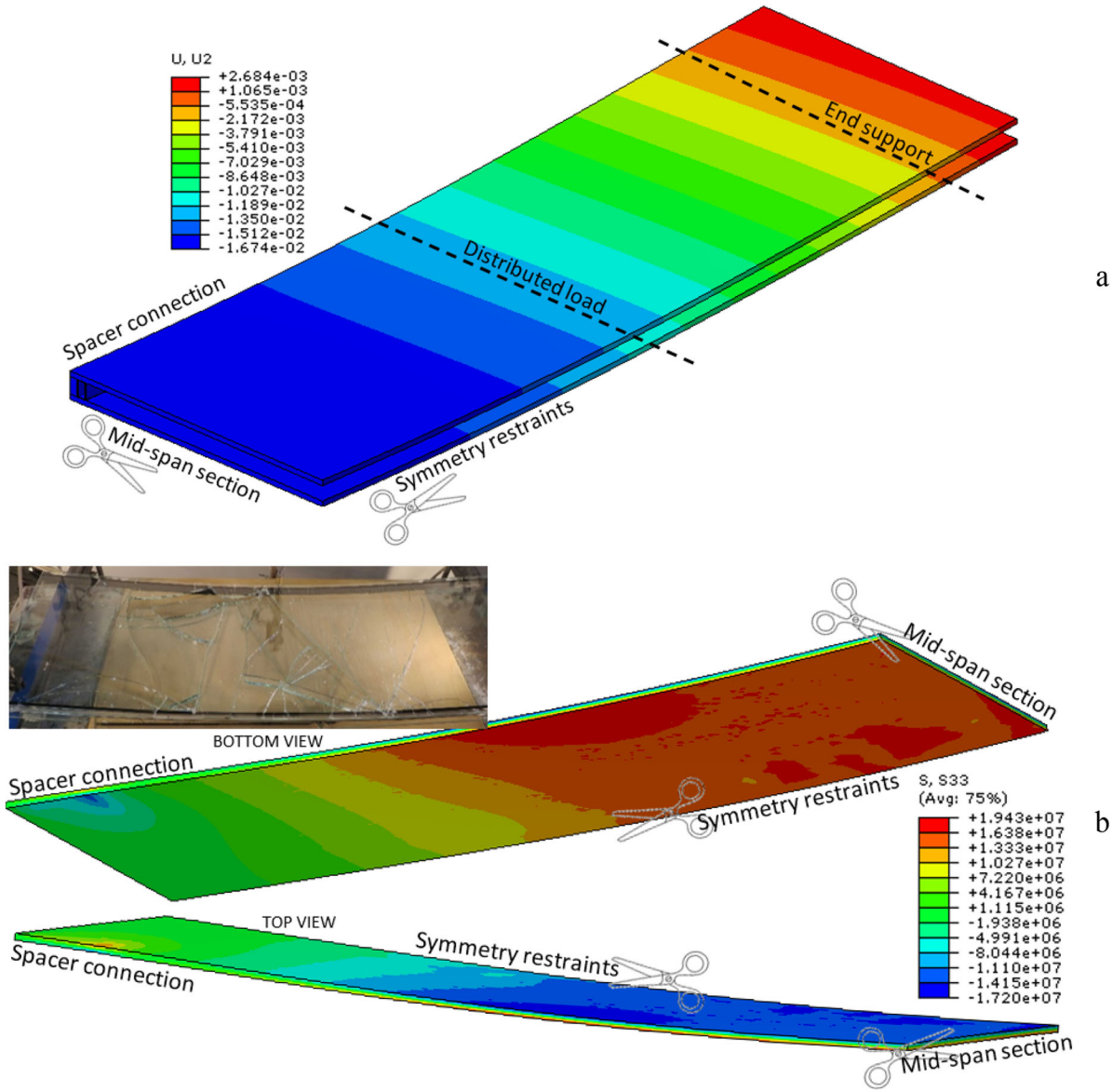

Fig. 7 Bending performance assessment of 2-edge sealed IGU panels (ABAQUS, with scale factor = 3): **a** typical beam-like deformation (displacement values in m) and **b** corresponding bi-triangular bending stress distribution in the glass panels (stress values in Pa)

contributions directly reflect on the stress distribution in each load-bearing member, glass panels included.

Given the relatively small aspect ratio and imposed test setup for the selected IGU panels, a typical beam-like bending performance was observed for them (see Fig. 7a). FE results are proposed for the FE-B1 system deprived of the silicone bonds. The relatively weak bonding effect offered by the spacer connections in use (AL bar + butyl) resulted in a bi-triangular distribution of stresses for both the glass panels (Fig. 7b). Maximum stress peaks were achieved in the region of load introduction, as in the case of most of the experimental specimens (see Bedon and Amadio 2020).

Fracture propagation and post-cracking performance for the selected IGU panels were both preliminary disregarded in the current FE study, given that the attention

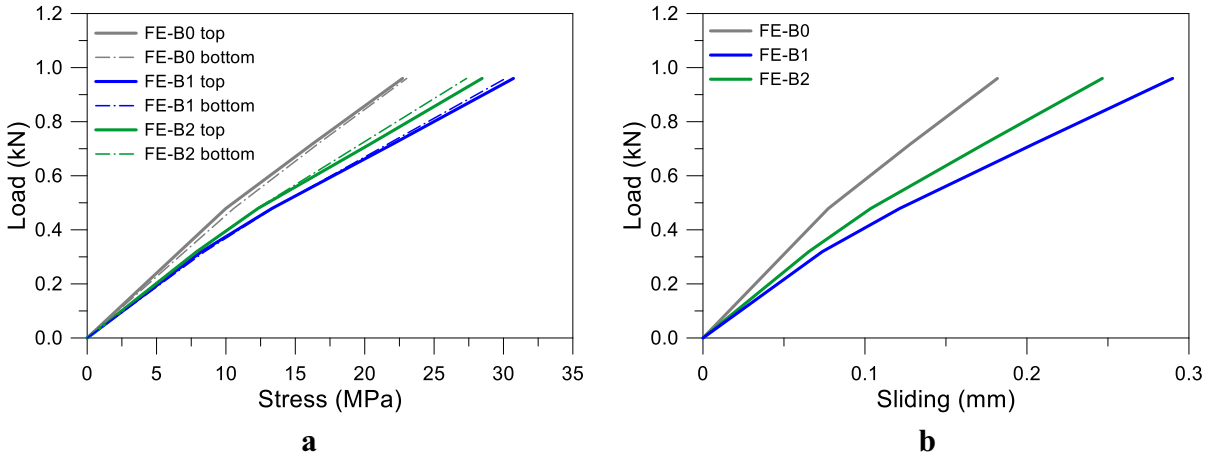

Fig. 8 Bending response of 2-edge sealed IGU panels (ABAQUS): **a** maximum envelope of tensile stresses along the restrained edges, as a function of the imposed load and **b** sliding of glass panels

was focused on the pre-cracked stage for glass. For all the FE models, however, stress peaks and evolution at different loading stages were in any case monitored, and compared with nominal resistance values for glass (45 MPa, for AN glass). Regarding the FE-B1 model in Fig. 7, for example a maximum tensile stress in the range of 20 MPa can be observed at an imposed deflection of ≈ 17 mm, that roughly corresponds to the collapse deformation for the 2C_01 sample with identical features.

Besides the global bending performance was observe to qualitative agree with Fig. 7 for all the investigated FE models, the primary effect of different mechanical properties for spacer connections was found in local effects emphasized in Fig. 8. For the FE-B0 model with a rather efficient bond, almost identical stress peaks along the glass edges were calculated for the top and bottom panels, with up to ≈ 20 MPa under 1 kN of total load (≈ 0.18 mm the relative sliding, see Fig. 8b). These stress peaks progressively increase—for the same load level of 1 kN—up to 25 MPa (+ 25%) and 30 MPa (+ 38%) for the FE-B2 and FE-B1 models respectively, and similar variations can be observed for the sliding values in Fig. 8b.

3.5 Analytical analysis of experimental and numerical estimates

As a further validation of the past experiments and FE numerical estimates, additional analytical calculations were carried out with the analytical models adapted from Möhler (1956) and Pascual et al. (2019) for sandwich sections respectively, and further discussed in Bedon and Amadio (2020).

The so-called γ-method from Möhler (1956), in particular, was used in Bedon and Amadio (2020) to extrapolate the spacer connection efficiency from the equivalent bending stiffness of each tested IGU specimen, i.e.:

$$(EI)_{y,eff} = \sum_{i=1}^{2} E_g I_{y,i} + \gamma \cdot \left(2E_g A_i \cdot z_i^2\right) + n_b \cdot \left(2EI_{y,bar}\right) + n_s \cdot \left(2EI_{y,sec}\right) \quad (6)$$

and thus

$$0 \le \gamma = \frac{(EI)_{y,eff} - \sum_{i=1}^{2} E_g I_{y,i} - n_b \cdot \left(2EI_{y,bar}\right) - n_s \cdot \left(2EI_{y,sec}\right)}{2E_g A_i \cdot z_i^2} \le 1 \quad (7)$$

with:

- E_g the modulus of elasticity of glass;
- $A_i = A = a \times h_i$ the cross-section of each glass layer ($i = 1, 2$);
- $I_{y,i} = (a \times h_i^3)/12$ the corresponding second moment of area ($i = 1, 2$);

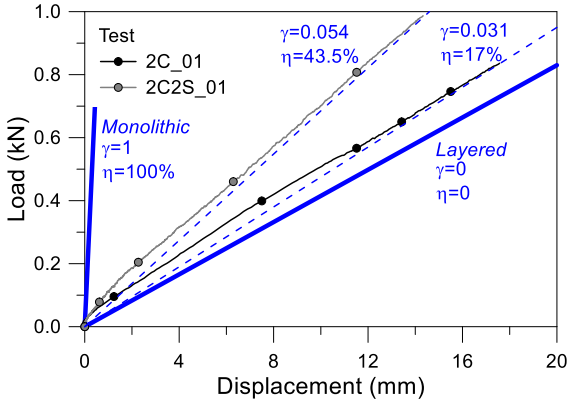

Fig. 9 Bending performance assessment of IGU panels (ABAQUS): analytical estimates of past experimental results (from Bedon and Amadio 2020)

- and z_i ($i = 1, 2$) the distance between the middle axis of each glass panel and the middle longitudinal axis for the IGU as a whole.

In the second case, see Pascual et al. (2019), the analytical formulation has been derived from the sandwich beam theory and well applies to the reference mechanical systems herein explored. Assuming that the bonding connection is ideally comprised between the *layered* ($\eta = 0$) and fully *monolithic* ($\eta = 100\%$) conditions, the connection efficiency parameter is in fact given by:

$$0 \leq \eta = \frac{w_{layered} - w}{w_{layered} - w_{monolithic}} 100 \leq 100\% \qquad (8)$$

with w the mid-span deformation of the system due to the actual bonding layers.

According to Fig. 6b, the adapted beam sandwich theory still offers a rather good correlation with the past load-deflection experimental estimates. Comparative analytical calculations are shown in Fig. 9. Moreover, it is possible to notice that the simple bonding connection given by butyl layers (2C series) can be associated to a degree of interaction in the order of $\eta = 17\%$ ($\gamma = 0.031$), and this is also in line with past experimental outcomes. Accordingly, the introduction of a bonded silicone layer (2C2S series) manifests in an increase up to ≈ 3 times the connection degree for the given geometry ($\eta = 43.5\%$). Such a beneficial contribution is overestimated in comparison to the γ-method, with $\gamma = 0.054$ for the 2C2S series (≈ 1.75 times the unsealed specimen).

4 FE numerical analysis of 4-edge sealed IGUs in bending

4.1 Methods

As a further extension of Sect. 3, the reference geometry and four-point bending test setup schematized in Fig. 5a was adapted to cover the geometrical configurations summarized in Table 5.

For the FE modelling stage, in addition to trivial geometrical variations, a special care was spent to account for the presence of a sealed cavity, and thus the related load sharing effects. A *fluid interaction* was in fact used in the cavity volume (pneumatic gas law), so that the effect of a possible interaction between the top and bottom glass panes could be numerically assessed.

To this aim, an initial FE step was defined before the four-point bending stage, in order to represent the cavity infill for the examined IGU specimens. At this stage, major efforts were thus spent for the definition of reliable cavity configurations. The sealing stage of IGUs (as well as the typical deformations of thermoplastic sealants under ordinary operational conditions) are in fact generally accepted to continuously change the cavity conditions. In the same way of temperature variations, ambient pressure changes can thus cause initial bending of glass panels that should be separately

Table 5 Four-point bending tests (group II, with $a = 300\,\text{mm} \times b = 1100\,\text{mm}$)

Series	Test repetitions	Label	h (mm)	Spacer bar	Seal type	Sealed edges in total	Secondary seal (n. of sealed edges), b_s (mm)
4C4S_AL	1 × 3 specimens	4C4S_AL01	10	AL	P + S	4	Y (4), 6
		4C4S_AL02	10	AL	P + S	4	Y (4), 6
		4C4S_AL03	10	AL	P + S	4	Y (4), 6

Key: *AL* aluminum, *WE* warm edge, *P* primary seal (Butylver 0.25 mm), *S* secondary seal (silicone DOWSIL 3363), *Y* yes, *X* no

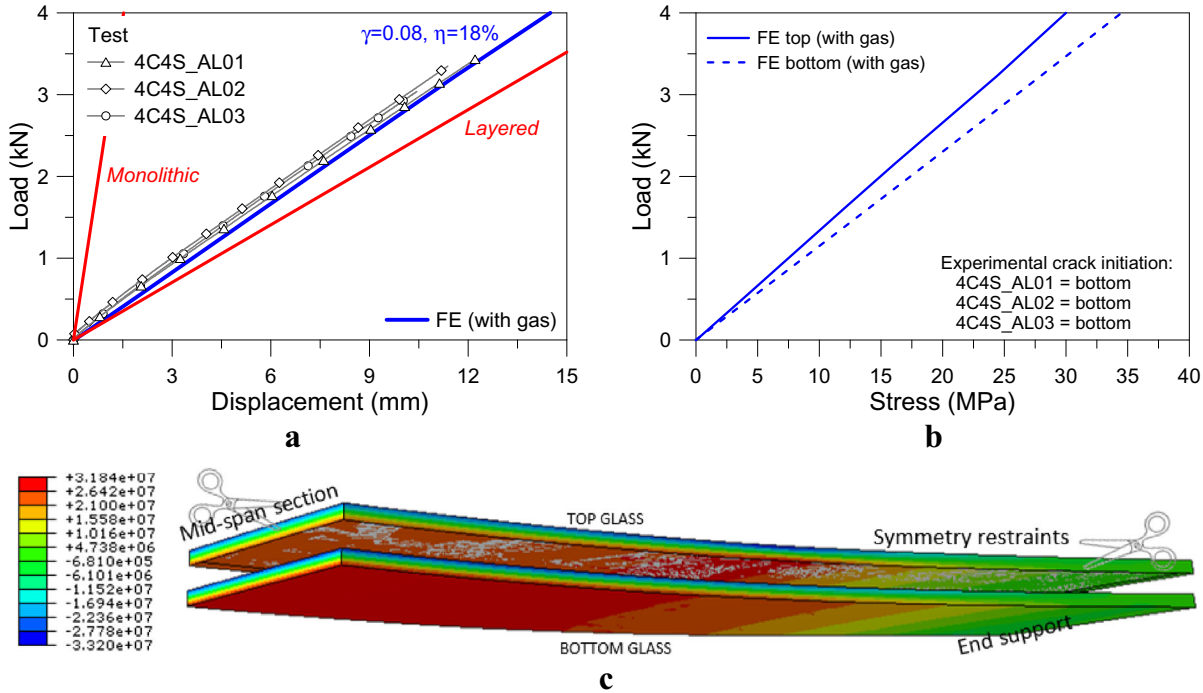

Fig. 10 Bending performance assessment of 4-edge sealed IGU panels (ABAQUS): **a** load-deflection, **b** load-tensile stress in glass, and **c** stress distribution in the glass panels (values in Pa). Experimental results reported from Bedon and Amadio (2020)

assessed (Koslowski and Wolf 2016), as an additional contribution leading to possible premature fracture of glass. All the other potential climatic effects (temperature, altitude, etc.) could then manifest in even further stress/deformation variations that should be combined with the external mechanical loads (wind, etc.).

In this research paper, the reference FE modelling assumption was to assume the worst possible atmospheric variation for the sealing stage of the examined IGUs, while disregarding additional climatic events (that should be separately assessed). In this sense, it is known that the common atmospheric pressure p_{amb} fluctuates in the range from $p_{min} = 0.95$ atm (low pressure) to $p_{max} = 1.03$ atm (high pressure), and thus both the limit conditions were taken into account to fill the FE gas cavity (Koslowski and Wolf 2016). A given IGU is in fact conventionally manufactured and sealed at a specific atmospheric pressure p_{seal} that falls in the above interval ($p_{min} \leq p_{seal} \leq p_{max}$). This means that a daily fluctuation of the ambient pressure p_{amb} unavoidably manifests in a certain imbalance with the internal cavity p_{seal} (with up to $\Delta p = \pm(p_{max} - p_{min}) = \pm 0.08$ atm, depending on the sealing conditions). The latter, accordingly, tends to flex the glass panels inward or outward, depending on p_{seal} and p_{atm}. Given the lack of specific details and measurements for the experimental specimens presented in Bedon and Amadio (2020), such a conservative FE assumption resulted respectively in an initial cavity over-pressure or under-pressure, compared to the external ambient, thus in a series of initial bending stress/deformations for the glass panels (due to pressure/volume variations in the cavity) that exhibited prior to the application of mechanical loads. For the examined geometrical configurations, the amount of these stress/deformation effects was generally found to be negligible (≈ 1 MPa of tensile stress at the mid-span section of glass), compared to the effects due to the four-point bending setup in use at the time of the destructive experiments.

4.2 Load-deflection and stress results

In general, the use of FE modelling approaches and input parameters according to Sect. 4.1 resulted in rather close correlation with the corresponding test measurements. In Fig. 10a, comparisons are shown in

terms of load-deflection estimates, for the reference FE model as well as for the limit layered and monolithic configurations. Besides the presence of 4-sealed edges and fully insulated IGU components, no sensitive variations were observed in comparison to the 2-edge sealed specimens discussed in Sect. 3. Accordingly, γ- and η-analytical estimates of connection efficiency resulted in ≈ 0.08 and $\approx 18\%$ respectively, thus further enforcing the presence of a relatively weak edge connection among the 10 mm thick glass panels.

As far as the stress evolution is investigated for the top and bottom glass panels, maximum tensile peaks were first numerically estimated for the bottom, unloaded panel, see Fig. 10b. Both the glass panes still proved to offer a beam-like bending distribution of tensile stresses (see also Fig. 10c). Under a total imposed load of 4 kN, stress peaks were predicted in the order of ≈ 27 MPa and ≈ 35 MPa for the top and bottom layers respectively, thus suggesting (as far as the variability of the actual resistance of glass specimens is disregarded) a fracture initiation from the bottom glass panel. Such a numerical outcome is also in line with the experimental observations reported in Bedon and Amadio (2020), where crack initiation was visually detected from the bottom glass panes of the three specimens belonging to the 4C4S series with AL spacer bar.

5 Load sharing effects and calculation example

At a final stage of the numerical investigation, the FE outcomes partly summarized in Sect. 4 were further elaborated, in order to develop useful comparative calculations with some analytical formulations, The attention was focused on the simplified analytical formulations currently in use to account for load sharing phenomena in glass panels belonging to IGUs under mechanical loads or climatic (internal) events (see for example prEN 13474-1 2007; CNR DT 210 2013).

Certainly, the IGU geometrical configurations investigated in this study may not be realistic for the description of full-scale load-bearing IGUs of practical use. In addition, it is important to remind that a detailed structural design process for IGU assemblies should generally take care of multiple aspects, namely the optimal thickness of glass, but also the detailing of spacer sealants under the expected operational conditions (see for example Dow Corning 2016; Wolf 2002, 2003). This is not the case of the calculation example herein reported, that preliminary focuses on the expected stress/displacement effects for the glass panels only, due to interposed edge connections and gas infills. In any case, the comparative results herein reported should represent a useful feedback for the reliability assessment of simplified design methods in use. The actually available load sharing formulations, see (prEN 13474-1 2007; CNR DT 210 2013), are in fact specifically recommended for IGUs with four linear supports along all the edges, and subjected to uniform distributed pressures. While these boundary and loading configurations are certainly of interest for design purposes, however, they do not reflect the high variability of possible operational conditions for IGUs in modern buildings.

As such, for comparative purposes, the 4C4S model in Fig. 10 was further explored in this paper, under the effects of a given uniformly distributed pressure $q = 2$ kPa, being imposed on the external glass surface of panel "1", see Fig. 11a. The latter can be representative of a short-time wind pressure acting on glass, or other short-term accidental loads. All the IGU geometrical features for global dimensions, glass thickness and spacer connection components were kept fix, as in the experimental investigation summarized in Sect. 4 and Bedon and Amadio (2020). Possible temperature/humidity variations were also disregarded in the calculation examples, so as to do not further affect the gas cavity (and thus involve additional potential initial stresses and deformations for the glass panels).

The comparative calculations were repeated for the same IGU geometry and imposed external pressure q, for the two different boundary conditions in Fig. 11b, c.

According to the (prEN 13474-1 2007; CNR DT 210 2013) technical documents, key parameters for load sharing effects in IGUs with linear supports along all the edges like Fig. 11b are:

$$k_1 = \frac{h_1^3}{h_1^3 + h_2^3} = 0.5 \; (for \; h_1 = h_2 = h) \tag{9}$$

$$k_2 = 1 - k_1 = 0.5 \tag{10}$$

with $i = 1$ for the exposed (loaded) glass panel and $i = 2$ the unexposed panel, while:

$$\varphi = \frac{1}{1 + \left(\frac{a}{a^*}\right)^4} = 0.908 \tag{11}$$

$$a^* = 28.9 \sqrt[4]{\frac{h_1^3 \, h_2^3 \, s}{(h_1^3 + h_2^3) \, k_5}} = 0.531 \tag{12}$$

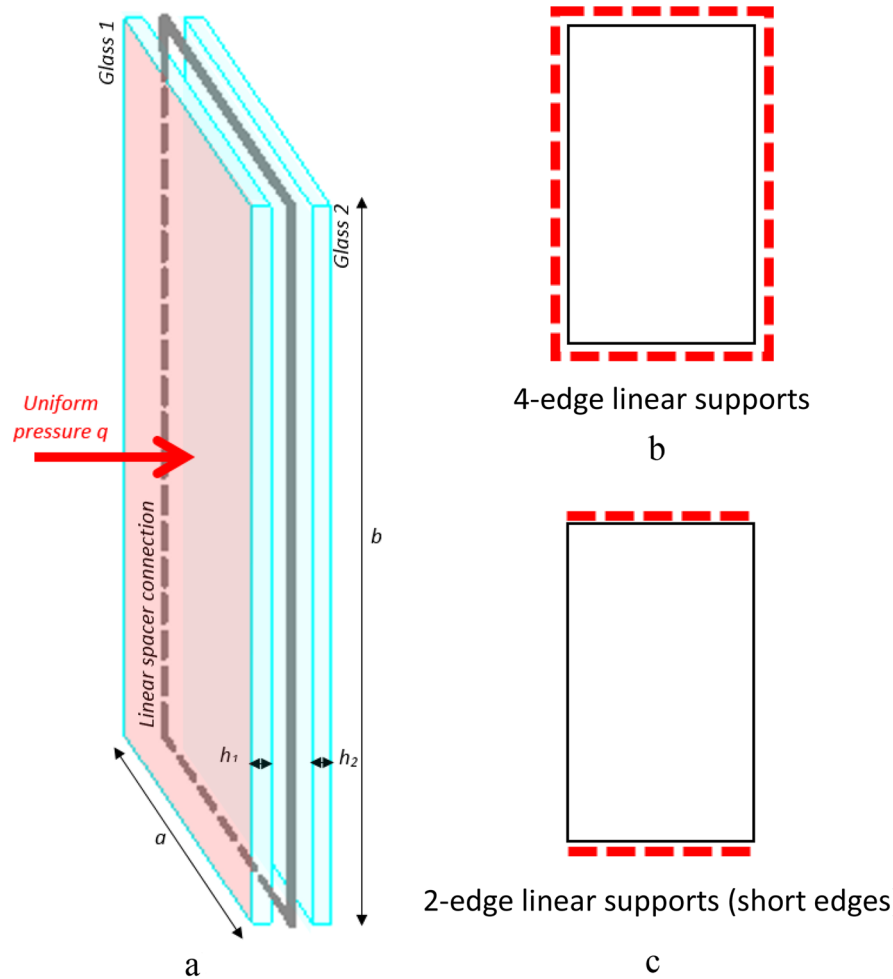

Fig. 11 Reference case-study system: **a** schematic representation of the whole geometry (with $a < b$), with **b**, **c** selected boundary conditions

where $\lambda = a/b = 300/1000 = 0.27$ and $k_5 = 0.07$ depends on the IGU aspect ratio λ.

Based on Eqs. (9)–(12), it follows that the imposed pressure q is expected to redistributes onto the two glass panels in the form of:

$$q_1 = (k_1 + \varphi\, k_2)\, q = 0.954q \tag{13}$$

$$q_2 = (1 - \varphi\,)\, k_2\, q = 0.046q \tag{14}$$

and thus most of the external pressure would be sustained by the external layer "1" only.

The conventional static calculation approach for the selected IGU requires then that the maximum tensile stresses and deformations due to the so calculated pressure contributions q_1 and q_2 are separately assessed for each layer. In other words, the minimum required thickness can be calculated for each panel as in the case of independent glass layers, under the effects of load contributions from Eqs. (13)–(14). Such a goal can be achieved with the support of non-linear analytical models agreeing with Table 6, where h is the thickness of glass plates and $A = a \times b$, with E the MoE of glass (while k_1 and k_4 are defined in the CNR DT 210 document as a function of the loading rate and λ).

The expressions recalled in Table 6 are known to offer reliable estimates for single monolithic (or even laminated, with equivalent thickness assumptions) glass plates under various boundary conditions.

Their reliability is also briefly emphasized in Table 7, where FE numerical and analytical calculations (from Table 6) are proposed for an independent, single monolithic glass panel under the loading and boundary conditions earlier schematized in Fig. 11 (with $h = 10$ mm the nominal thickness). For a given glass plates with both 4 or 2 linear edge supports and uniform pressure q, the rather good correlation of stress and deflection estimates can be perceived from Table 7.

Table 6 Analytical model for rectangular glass panels under distributed design pressure (CNR DT 210/2013)

Parameter	4 linear supports Fig. 11b	2 linear supports (short edges restrained) Fig. 11c
Stress	$\sigma_{max} = k_1 \frac{A}{h^2} q_i$	$\sigma_{max} = 0.75 \frac{b^2}{h^2} \frac{q_i}{E}$
Displacement	$w_{max} = k_4 \frac{A^2}{h^3} \frac{q_i}{E}$	$w_{max} = 0.148 \frac{b^4}{h^3} \frac{q_i}{E}$

Table 7 Numerical and analytical stress/displacement estimates for a single glass panel ($h = 10$ mm) under a $q = 2$ kPa distributed pressure

	4 linear supports Fig. 11b Independent, single glass panel (legend values in m)		2 linear suppoorts (short edges restrained) Fig. 11c Independent, single glass panel (legend values in m)	
	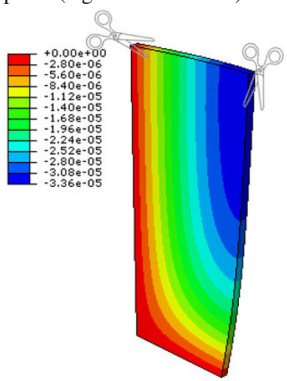		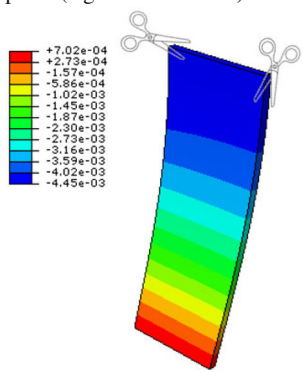	
	FE numerical (ABAQUS)	Analytical (Table 6)	FE numerical (ABAQUS)	Analytical (Table 6)
Stress (MPa)	1.32	1.32	15.10	15.00
Displacement (mm)	0.04	0.04	4.45	4.23

Major issues, on the other side, arise from the analysis of IGUs under the above loading and boundary conditions. As far as static calculations are extended to composite IGUs, stress/deflection estimates can in fact take advantage of Eqs. (9)–(14) for 4-edge linearly supported panels. In contrary, 2-edge linearly supported IGUs still suffer from the availability of dedicated (and reliable) load sharing analytical models.

For comparative purposes, FE and analytical IGU predictions are thus reported in Table 8. The collected FE results, as also in accordance with previous experimental validations, generally gave evidence of a rather uniform redistribution of load effects onto both the exposed (loaded) and unexposed (unloaded) glass panels. Besides that, a more detailed analysis of the bending response for the single glass layers composing the IGU was found to be still in line with the contour plots in Table 7. More in detail, see Table 8, a close correlation can be observed in the stress/displacement response of the 4-edge linearly supported IGU (for both the glass panels), with respect to the analytical predictions of Eqs. (9)–(14) and Table 6.

In the case of 2 linearly restrained edges, otherwise, no analytical feedback is available from the existing load sharing analytical approach. The bending response was found to agree with the experimental outcomes reported in Sect. 4. Accordingly, Table 8 shows that stress and displacement effects in glass are rather uniformly distributed on both the exposed and unexposed glass panels, with mostly identical effects due to the external pressure q, that roughly corresponds to $q_1 = q_2 \approx 0.5q$. Such an effect can be primarily explained in the global bending deformation of the two reference configurations, namely a plate (for the 4-edge supported) and a beam-like (2-edge supported) behaviour, and thus on the actual bending contribution of the spacer bars in use. In the second case, more in detail, the bars themselves are subjected to relevant

Table 8 Numerical and analytical stress/displacement estimates for the selected case-study IGU under a $q = 2$ kPa distributed pressure

	4-edge linear supports Fig. 11b				2-edge linear suppoorts (short edges restrained) Fig. 11c			
	Glass 1 (exposed)		Glass 2 (unexposed)		Glass 1 (exposed)		Glass 2 (unexposed)	
	FE numerical (ABAQUS)	Analytical (Table 6)	FE numerical (ABAQUS)	Analytical (Table 6)	FE numerical (ABAQUS)	Analytical (Table 6)	FE numerical (ABAQUS)	Analytical (Table 6)
Stress (MPa)	1.09	1.26	0.058	0.061	4.90	x	4.92	x
Displacement (mm)	0.038	0.04	0.002	0.002	1.96	x	1.89	x

bending deformations, due to the lack of continuous restraints along the longest edges. As far as the spacer connection is able to carry on the external loads, it follows that the unexposed glass panel is forced to bend in the same way of the loaded glass panel, thus to attain large deformations and high stress peaks.

For the same boundary condition, moreover, pressure/volume variations in the gas cavity (still occurring) were indeed found to have a minor contribution, compared to the typical load sharing phenomena that are generally expected in IGUs with 4-edge linear supports. In order to further generalize such a kind of effect, however, further extended studies should be dedicated to IGUs with similar loading/boundary conditions and characterized by a high variability of geometrical features (i.e., aspect ratio λ, glass thickness h, cavity thickness s, etc.) or mechanical characteristics (i.e., spacer connection components, size, materials), as well as loading conditions (including long-term effects or ambient variations). Finally, a separate care should be dedicated to the analysis of triple glass units with two gas cavities, in which the above outcomes are expected to further magnify.

6 Conclusions

Insulated Glass Units (IGUs) are largely used in buildings, due to a series of motivations. Among others, IGUs can be involved as mechanical systems able to behave as composite assemblies characterized by the presence of linear connections along their edges. As such, dedicated methods of analysis and design are conventionally required to capture their actual mechanical performance, first of all the well-known load sharing effects.

This paper further extended a previous research study ("Part I"), in which the mechanical response of IGU specimens under shear and bending was experimentally investigated. Careful consideration was paid for the shear performance assessment of silicone sealed spacer connections of typical use for IGUs, as well as on the bending performance of IGU prototypes with two linearly supported edges.

Based on the past experimental outcomes, in particular, accurate Finite Element numerical models have been presented to explore the load-bearing performance of selected configurations of spacer connections and IGU geometries. A focus was spent on the

actual mechanical contribution of primary and secondary seals, and on how they can both contribute to the final stiffness and resistance of IGU assemblies.

Taking further advantage of FE numerical models validated towards past experiments, final efforts were dedicated to the preliminary assessment of analytical models that are in use to account for load sharing phenomena in IGUs. Among others, the European standards formulations are sensitive to the size of a given IGU to verify, as well as to the thickness of the constituent glass panels, and the thickness of the interposed gas cavity. Especially for IGUs with relatively small slenderness ratio, in addition, the latter results in load sharing phenomena that are mostly conservative for the glass plate that is exposed to the assigned external loads, while disregarding possible load sharing effects for the unexposed glass panel. Moreover, the standardized analytical approach for load sharing effects is suitable for IGUs with four linearly supported edges, and cannot be adapted to other boundary conditions of technical interest (i.e., 2-edge restrained assemblies, etc.). As such, simple analytical calculations of literature that actually support IGU designers are specifically intended for assemblies with a plate behaviour, rather than a beam-like response under the design mechanical or climatic loads.

According to the collected FE and analytical predictions, it was shown in this paper that even in the case of 2-edge supported, beam-like IGUs, both the spacer connection features and the interposed gas infill can be still responsible od a coupled mechanical interaction for both the constituent glass panels in use, thus resulting in a relatively balanced redistribution of design loads and thus in similar stress/strain estimates for the glass layers to design. Such an effect mostly depends on the bending deformation of the spacer bars along the unrestrained IGU edges. As far as the spacer connection components are able to carry on the imposed loads, it turns out that the unexposed glass panel is forced to flex in the same way of the loaded glass plate.

At the same time, besides the research outcomes reported herein, it is also recognized that further influencing parameters should be further assessed for IGUs or even Triple TGUs, including a combination of mechanical variations and also various operational conditions (i.e., long-term phenomena, climatic loads, etc.) of technical interest. The actual comparative results and conclusions, accordingly, will be further extended towards the assessment of simplified analytical models in use for IGU assemblies under various boundary conditions.

Acknowledgements Ing. Pasquale Lucia (BLDing Studio, www.blding.it) and Zanatta Vetro S.p.A. (www.zanattavetro.it) are acknowledged for providing the IGU specimens. A special thanks for Ing. Franco Trevisan (University of Trieste), for the technical support during the whole experimental investigation. Finally, Ing. Irene Panizzut is acknowledged for her collaboration.

Compliance with ethical standards

Conflict of interest The authors declare that there are no conflicts of interest regarding the publication of this paper.

References

Bedon, C.: Issues on the vibration analysis of in-service laminated glass structures: analytical, experimental and numerical investigations on delaminated beams. Appl. Sci. **9**, 3928 (2019). https://doi.org/10.3390/app9183928

Bedon, C., Amadio, C.: Mechanical analysis and characterization of IGUs with different silicone sealed spacer connections—part 1: experiments. Glass Struct. Eng.*under review* (2020). https://link.springer.com/article/10.1007/s40940-020-00122-w

Bedon, C., Amadio, C.: A linear formulation for the ULS design of glass elements under combined loads: application to IGUs. Glass Struct. Eng. **3**(2), 289–301 (2018a)

Bedon, C., Amadio, C.: Buckling analysis and design proposal for 2-side supported double insulated glass units (IGUs) in compression. Eng. Struct. **168**, 23–34 (2018b)

Bedon, C., Machalická, K., Eliášová, M., Vokáč, M.: Numerical modelling of adhesive connections including cohesive damage. Chall. Glass Conf. Proc. **6**, 303–320 (2018). https://doi.org/10.7480/cgc.6.2155

Buddenberg, S., Hof, P., Oechsner, M.: Climate loads in insulating glass units: comparison of theory and experimental results. Glass Struct. Eng. **1**, 301–313 (2016)

CNR DT 210: Istruzioni per la progettazione, l'esecuzione e il controllo di costruzioni con elementi strutturali di vetro. Consiglio Nazionale delle Ricerche, Roma, Italy. www.cnr.it (2013)

Dow Corning.: Insulating Glass Quality Manual (39 pages) (2016)

Dural, E.: Analysis of delaminated glass beams subjected to different boundary conditions. Compos. Part B Eng. **101**, 132–146 (2016)

EN 485-2.: Aluminium and aluminium alloys—Sheet, strip and plate—Part 2: mechanical properties. CEN - European Committee for Standardization, Brussels, Belgium (2016)

EN 572-2.: Glass in buildings—basic soda lime silicate glass products. CEN - European Committee for Standardization, Brussels, Belgium (2004)

EN 573-3.: Aluminium and aluminium alloys—chemical composition and form of wrought products—part 3: chemical

composition and form of products. CEN - European Committee for Standardization, Brussels, Belgium (2019)
EN 10088-2.: Stainless steels—part 2: technical delivery conditions for sheet/plate and strip of corrosion resisting steels for general purposes. CEN - European Committee for Standardization, Brussels, Belgium (2014)
Haldimann, M., Luible, A., Overend, M.: Structural Use of Glass; IABSE – International Association for Bridge and Structural Engineering: Zurich, Switzerland; ISBN 978-3-85748-119-2 (2008)
Hänig, J., Bukieda, P., Engelmann, M., Stelzer, I., Weller, B.: Examination of laminated glass with stiff interlayers–numerical and experimental research. Int. J. Struct. Glass Adv. Mater. Res. **3**, 1–14 (2019). https://doi.org/10.3844/sgamrsp.2019.1.14
Katsivalis, I., Thomsen, O.T., Feih, S., Achintha, M.: Development of cohesive zone models for the prediction of damage and failure of glass/steel adhesive joints. Int. J. Adhes. Adhes. **97**, 102479 (2019)
Koslowski, J., Wolf., T.A.: Sealants in Construction. CRC Press, ISBN: 978-1-4200-1785-4 (eBook) (2016)
Kuntsche, J., Schuster, M., Schneider, J.: Engineering design of laminated safety glass considering the shear coupling: a review. Glass Struct. Eng. **4**, 298–328 (2019)
Liang, R.F., Mackley, M.R.: Rheological characterization of the time and strain dependence for polyisobutylene solutions. J. Non-Newton. Fluid Mech. **52**, 387–405 (1994)
Machalicka, K., Eliasova, M.: Adhesive joints in glass structures: effects of various materials in the connection, thickness of the adhesive layer, and ageing. Int. J. Adhe. Adhes. **72**, 10–22 (2016)
McMahon, S., Norville, H.S., Morse, S.M.: Experimental investigation of load sharing in insulating glass units. J. Arch. Eng. **24**(1), 04017038 (2018)
Möhler, K.: Über das Verhalten von Biegeträgern und Druckstäben mit zusammengesetzten Querschnitten und nachgiebigen Verbindungsmitte, TH Karlsruhe (1956)
Morse, S.M., Norville, H.S.: Comparison of methods to determine load sharing of insulating glass units for environmental loads. Glass Struct. Eng. **1**(1), 315–329 (2016)
Pascual, C., Montali, J., Overend, M.: Adhesively-bonded GFRP-glass sandwich components for structurally efficient glazing applications. Compos. Struct. **160**, 560–573 (2019)
prEN 13474-1: Glass in building—design of glass panes—part 1: general basis of design. CEN - European Committee for Standardization, Brussels, Belgium (2007)
Sharma, A.K., Bhattacharya, B.: Parameter estimation of butyl rubber aided with dynamic mechanical analysis for numerical modelling of an air-inflated torus and experimental validation using 3D-laser Doppler vibrometer. J. Low Freq. Noise Vib. Active Control **38**(2), 296–311 (2019). https://doi.org/10.1177/1461348419825685
Simulia: ABAQUS Computer Software. Dassault Systemes, Providence (2020)
Starman, B., Macek, A., Rus, P., Obid, S., Kralj, A., Halilovic, M.: Primary seal deformation in multipane glazing units. Appl. Sci. **10**, 1390 (2020). https://doi.org/10.3390/app10041390
Turowec, B.A., Gillies, E.R.: Synthesis, properties and degradation of polyisobutylene–polyester graft copolymers. Polym. Int. **66**(1), 42–51 (2016)
Wolf, A.T.: Design and material selection factors that influence the service-life and utility value of dual-sealed insulating glass units. Dow Corning Paper 106, 10 pages (2002)
Wolf, A.T.: Silicone sealed Insulating Glass Units. In: Proceedings of Glass processing Days (2003)